

Better audio representations are more brain-like: linking model-brain alignment with performance in downstream auditory tasks

Leonardo Pepino^{1,2}, Pablo Riera^{1,2}, Juan Kamienkowski^{1,2},
Luciana Ferrer¹

¹Instituto de Investigación en Ciencias de la Computación (ICC),
CONICET-UBA, Argentina.

²Departamento de Computación, FCEyN, Universidad de Buenos Aires
(UBA), Argentina.

Contributing authors: lpepino@dc.uba.ar; priera@dc.uba.ar;
juank@dc.uba.ar; lferrer@dc.uba.ar;

Abstract

Artificial neural networks (ANNs) are increasingly powerful models of brain computation, yet it remains unclear whether improving their task performance also makes their internal representations more similar to brain signals. To address this question in the auditory domain, we quantified the alignment between the internal representations of 36 different audio models and brain activity from two independent fMRI datasets. Using voxel-wise and component-wise regression, and representation similarity analysis (RSA), we found that recent self-supervised audio models with strong performance in diverse downstream tasks are better predictors of auditory cortex activity than older and more specialized models. To assess the quality of the audio representations, we evaluated these models in 6 auditory tasks from the HEAREval benchmark, spanning music, speech, and environmental sounds. This revealed strong positive Pearson correlations ($r > 0.7$) between a model's overall task performance and its alignment with brain representations. Finally, we analyzed the evolution of the similarity between audio and brain representations during the pretraining of EnCodecMAE. We discovered that brain similarity increases progressively and emerges early during pretraining, despite the model not being explicitly optimized for this objective. This suggests that brain-like representations can be an emergent byproduct of learning to reconstruct missing information from naturalistic audio data.

Keywords: auditory models, neuroconnectionism, representation similarity analysis, fMRI

1 Introduction

Artificial Neural Networks (ANN) are currently among the most promising models of brain computation, replicating several core properties of biological systems [1]. As these models continue to excel at tasks traditionally associated with human intelligence, a central question arises: do their internal representations mirror those found in biological neural systems? Prior work has investigated this question across multiple domains, including vision [2–7], language [8–11], and audition [12–16]. These studies have shown that representations from deep neural networks (DNNs) can predict brain activity sometimes better than classical models designed to mimic human perception and cognition. A correspondence has also been observed between the hierarchical structure of DNNs and the organization of cortical processing stages. For example, Güçlü and van Gerven [2] found that early layers of a convolutional neural network (CNN) best predict activity in primary visual cortex (V1), while deeper layers more accurately predict responses in higher-level visual areas such as the lateral occipital complex (LOC), which is involved in object recognition. Similar correspondences have been reported for video stimuli [5], auditory stimuli [16], and text [17].

Another question that arises is: as models get better at solving everyday tasks, do their representations also become more similar to our brain representations? Prior work [11], has shown that as language models are more capable of predicting the next word in a text, the alignment between their representations and those derived from brain activity increases. Also, it has been shown that aligning representations with brain data leads to better performance in downstream tasks [18, 19]. These results support the Platonic Representation Hypothesis [20], which proposes that different models trained on different sensory modalities converge toward a shared, modality-agnostic “Platonic” representation of reality. Empirical evidence for this hypothesis comes from analyses showing that the similarity (e.g., centered kernel alignment, CKA) between representations of models pretrained on text and images increases as these models improve. One possible explanation is that as models become more general and capable of solving diverse tasks, the space of representations that can simultaneously support these tasks becomes increasingly constrained. Consequently, since the tasks that the artificial systems are trained to optimize overlap with those biological systems learn to solve, it is plausible that artificial and biological systems converge toward similar representations.

In this work, we tested these ideas in the auditory domain, focusing on deep neural networks trained for audio-related tasks, and linking downstream performance with brain similarity for the first time in this domain. We first analysed the similarity between 36 different audio models and representations derived from 2 fMRI datasets consisting of recordings of the auditory cortex collected during naturalistic listening of 165 different auditory stimuli. We selected a diverse set of audio models, spanning models specialized to solve particular tasks, which have been analysed in previous

works [16], and more recent and performant self-supervised general audio representations based on transformers [21–23]. From this first analysis we collected metrics of similarity between the audio and brain representations, derived using 3 different techniques: RSA, voxel and fMRI components regression. In addition to these similarity metrics, we performed a downstream evaluation of the audio models in 6 diverse auditory tasks spanning music, speech and environmental sounds understanding. Given this collection of metrics for the 36 audio models under analysis, we aimed to answer several research questions:

1. Do better audio models lead to more brain-like representations? We compared the performance metrics obtained by evaluating the representations in downstream auditory tasks with the brain-similarity metrics obtained using RSA and regression of the fMRI recordings. Our results show that models which perform better on a variety of downstream audio tasks like acoustic event detection and music genre classification, also exhibit stronger alignment with auditory cortical responses. This echoes similar findings in the language domain [8] and suggests that optimizing for human-relevant tasks may promote brain-like representations.
2. Are modern self-supervised audio models better aligned with brain? We incorporated recent state-of-the-art audio models: BEATs [21], Dasheng [22], and EnCodecMAE [23], which were trained using masked language modeling across diverse audio domains (speech, music and environmental sounds), and were not analysed through the lens of brain similarity in previous works. Our results show that these models are better predictors of fMRI recordings than less recent audio models that were optimized in a single domain like speech or for a single task like automatic speech recognition (ASR)
3. What are the factors that make a model’s representations more or less similar to the brain activity? By strategically selecting models with controlled variations, we isolate specific factors to measure their impact on alignment, such as model size, training data diversity, pretraining objectives, and architectural choices. For example, we compare the same model pre-trained on different audio domains (speech, music or both).
4. How does the similarity with the brain evolve during pretraining? We show that brain similarity increases progressively during the self-supervised pretraining of EnCodecMAE, despite not being explicitly involved in the optimization objective. This provides further evidence that alignment with the brain may emerge naturally when learning from naturalistic data and reconstructing missing information.

Together, these analyses allow us to test hypotheses about which model characteristics yield representations most aligned with the human auditory cortex. In particular, we find that the models that perform better on downstream tasks tend to align better with the brain. These models utilize a self-supervised learning objective where they are trained to restore missing information in audio signals, specifically by predicting masked audio segments from diverse auditory contexts. This training objective is consistent with theories of predictive coding and its role in auditory perception and language learning [24], which might explain the resulting representational alignment. For example, when these self-supervised models are trained on speech-only data, their

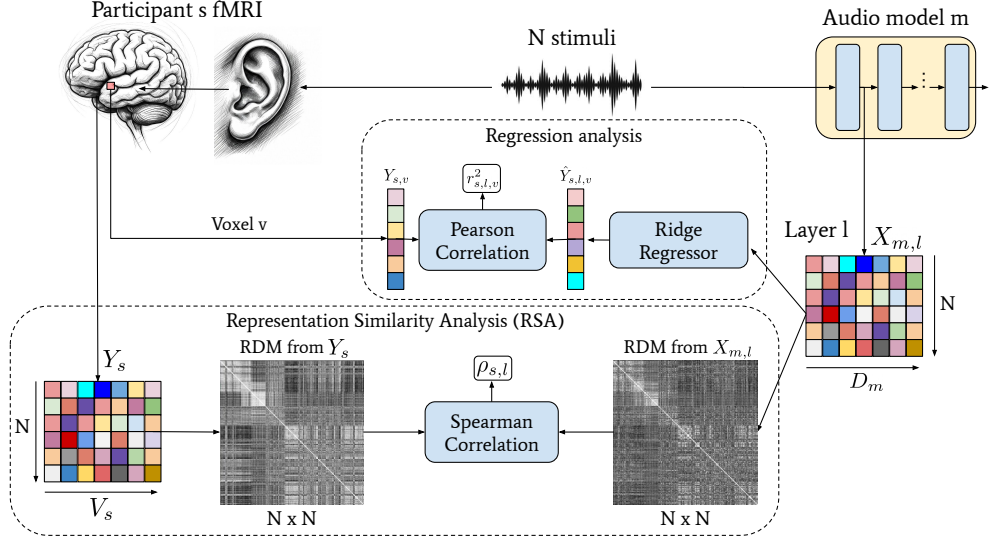


Fig. 1 Schematic depicting the two main analysis we performed to compare audio and brain representations: regression analysis and representation similarity analysis (RSA). For regression, the target variable is the fMRI activity $Y_{s,v}$ of a voxel v and subject s and the predictor variable is the activation map $X_{m,l}$ from layer l of an audio model m . For RSA, RDM matrices are calculated from $X_{m,l}$ and all the voxels from a subject Y_s and compared using Spearman Correlation.

objective is analogue to phonemic restoration [25], where missing segments of speech are restored by the brain, and the listener might not even notice that there are missing phonemes.

To our knowledge, this is the first study to systematically link brain alignment with downstream audio performance across a wide range of audio and speech models, and to analyze the evolution of similarity along the model pretraining process. These findings provide new insight into how task optimization, input representations, and training signals shape the alignment between artificial and biological neural representations.

2 Results

An overview of the analyses we performed in this study is summarized in Figure 1. The main goal of these analyses is to get a measure of the similarity between audio and brain representations when presented with auditory stimuli. The two analysis techniques we used for measuring this similarity are regression and representation similarity. In the regression analysis, for each voxel v and subject s , a ridge regressor is trained to predict the summarized fMRI activity of all $N = 165$ presented auditory stimuli, collected into a vector $Y_{s,v}$, from the audio representations of model m and layer l , $X_{m,l}$ for the same N stimuli. The Pearson correlation r between the estimated and ground truth fMRI activity is used as a measure of alignment between the representations $Y_{s,v}$ and $X_{m,l}$. In the Representation Similarity Analysis (RSA), for each subject s , the summarized fMRI activity for all stimuli and voxels is collected into a

matrix Y_s of size $N \times V_s$, where V_s is the number of voxel for subject s . This representation is compared with the audio representation $X_{m,l}$ by computing the Spearman correlation coefficient, $\rho_{m,s,l}$, between the corresponding representation dissimilarity matrices (RDM).

We evaluated the alignment between brain and model representations using two independent fMRI datasets: NH2015 [26] and B2021 [27]. These datasets capture BOLD responses in the auditory cortex of human participants as they listened to natural sounds. In each dataset, participants completed three scanning sessions where they heard the same $N = 165$ two-second audio clips corresponding to everyday natural sounds. NH2015 includes data from 8 participants with moderate musical training, while B2021 includes 20 different participants divided equally into two groups: one with minimal formal musical experience, and one with extensive musical training. Details on fMRI acquisition and pre-processing are provided in Section 4.1.

We extracted activations $X_{m,l}$ from 36 different audio models, combining those analysed in Tuckute et al. [16] with three recent self-supervised audio models: BEATs [21], Dasheng [22], and EnCodecMAE [23]. These models were trained on large-scale unlabeled audio using masked language modeling (MLM), a task in which the model learns to reconstruct masked segments of the input from context. They have achieved strong performance across diverse tasks involving speech, music, and environmental sounds. For each model, we extracted intermediate representations by running a forward pass over all 165 audio stimuli. Full details on model configurations and feature extraction procedures are available in Section 4.2.

2.1 Audio models can predict fMRI responses in auditory cortex

In our first analysis, we compare the representations from 36 audio models (see Section 4.2 for more details) in terms of their overall ability to predict fMRI representations using linear regression. The set of 36 models incorporates those already analysed in Tuckute et al. [16] as well as more recent models like EnCodecMAE, BEATs and Dasheng, which are trained with self-supervision and diverse auditory signals. As shown in Figure 1, for the regression analysis we trained L2-regularized (ridge) linear regressors to predict a vector $Y_{s,v}$ of length N corresponding to the activity in voxel v of subject s when listening to the N stimuli. We used the audio representations $X_{m,l}$ from layer l of model m as input features, and searched the best layer l and regularization weight α , for each voxel predictor, $Y_{s,v}$, using nested cross-validation on 5 equal-size splits balanced by stimuli type. This way, for each voxel v and subject s we obtained predictions $\hat{Y}_{s,v}$ that we compared with $Y_{s,v}$ using the Pearson determination coefficient, resulting in a matrix $R^2_{m,s,v}$. Then, we computed the median of $R^2_{m,s,v}$ across the voxels of each subject, obtaining $R^2_{m,s}$. Finally, we computed the mean across subjects, leading to a single summary metric, R^2_m , for how well model m can predict brain activity.

For models with a large number of layers, we evaluated only a subset of evenly spaced layers instead of computing alignment for all of them. This decreases the computational cost of the analysis and ensures a more fair comparison across models of varying depth, since approximately the same number of layers are evaluated for all

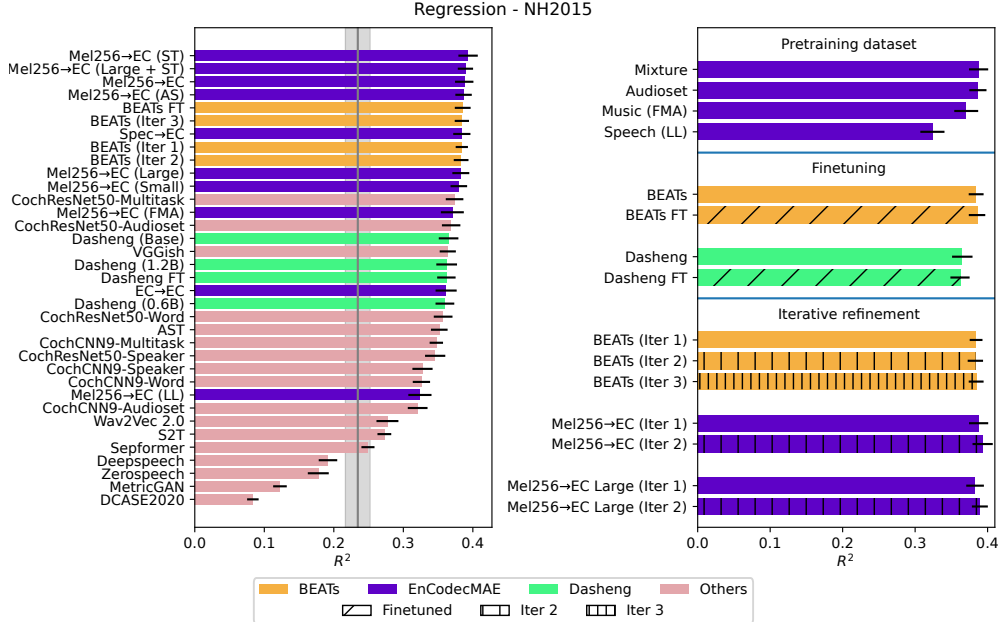


Fig. 2 Left: R^2 obtained for the analyzed audio models. Right: same results as in left, selecting groups of systems to highlight various interesting conclusions discussed in the text. The gray line corresponds to a spectro-temporal baseline system, and error bars reflect the standard error measured across subjects.

models when choosing the best layer during nested-cross-validation. Specifically, for the Large versions of EnCodecMAE, we used the odd-numbered layers (1, 3, 5, ..., 19) and the final layer. For Dasheng 0.6B and 1.2B, we sampled every fourth layer (1, 5, 9, 13, ..., K), with $K = 29$ for Dasheng 0.6B and $K = 37$ for Dasheng 1.2B, and included the final layer in both cases (32 for Dasheng 0.6B and 40 for Dasheng 1.2B).

Figure 2 (left) shows the results obtained for the different models. The recent audio models pretrained with self-supervision in diverse audio (EnCodecMAE, BEATs and Dasheng), outperform more specialized models analysed in previous works (shown in pink bars). This suggests that more recent models, achieving stronger performance in general audio tasks, are also better predictors of the auditory cortex activity. Several noteworthy findings, shown in more detail in Figure 2 (right), include:

- **Pretraining data plays a key role.** When EnCodecMAE is trained only on clean speech (LibriLight), its alignment with brain representations is considerably lower than when trained on musical signals (FMA) or on a mixture of music, environmental sounds, and clean speech (Audioset and Mixture). In particular, models trained on mixtures of diverse audio sources show the strongest prediction capabilities. One possible explanation for Dasheng's relatively poorer alignment compared to the other recent models, despite being a high-performing model in downstream tasks, is that its pretraining dataset is composed mainly (96.6%) of the ACACV100M dataset [28]. This dataset was constructed by selecting YouTube videos with high

mutual information between audio and visual signals. As a result, events where sound and image are tightly coupled – such as frontal speech or musical performances – are overrepresented, while background sounds such as ambient noise, background speech, rain, or music may be underrepresented. This selection bias may result in a model that aligns less well to brain signals for being less representative of the data to which humans are commonly exposed.

- **Finetuning on acoustic event detection does not seem to improve alignment with auditory cortical representations.** Recent works suggest that instruction finetuning [29] or training models for specific tasks [30] lead to a better alignment between models and brain representations. In this case, we do not observe any significant difference between the checkpoints finetuned for acoustic event detection, and the ones that were not finetuned for a specific task. This also shows that the masked language modelling task already achieves representations that are aligned with the brain, without the need for training on a specific task.
- **No clear effect of iterative refinement of targets in audio-brain alignment.** Although it's been shown that the iterative refinement of targets in certain models like HuBERT plays an essential role in improving its representations and changes its organization across layers [31], we do not observe significant changes in the alignment to brain representations.

2.2 Similar conclusions from Representation Similarity Analysis

Additionally, as depicted in Figure 1, we performed a similarity analysis between representations from audio models and fMRI recordings. We computed representational dissimilarity matrices (RDM) for $X_{m,l}$ and Y_s , and compared both RDMs by calculating the Spearman correlation coefficient between their flattened lower triangular matrices. As further explained in Section 4.5, the elements of the RDMs are calculated as one minus the Pearson correlation coefficient between the representations for every pair of stimuli, given by the rows in the input matrix, Y_s or $X_{m,l}$. In Figure 3, the RDM from the 4th layer of Mel256→EC (Large) and the RDM from fMRI measurements of one subject are shown. As can be seen, both RDMs exhibit similar structure, with higher similarity (lighter colors) observed between stimuli of the same type. For example, some instrumental music stimuli show strong internal dissimilarity (darker bands in the upper-left corner) in both the fMRI data and the representations from layer 4 of EnCodecMAE. In order to compare these dissimilarity matrices, we calculated the Spearman correlation coefficient, $\rho_{m,l,s}$. Finally, to obtain a single value per model m , we averaged those values across subjects and then took the maximum across layers. We call this number the RSA coefficient, ρ_m . We also tried performing cross-validation on the RDMs so that the best layer is selected on held-out data, but the results were very similar (see section 4.5).

As shown in Figure 4, consistent with the regression analysis in Section 2.1, pretraining with diverse data (Mel256→EC and Mel256→EC (AS)) leads to representations more similar to brain activity, as measured by the RSA coefficient, than models pretrained with domain-specific data like music (Mel256→EC (FMA)) and speech

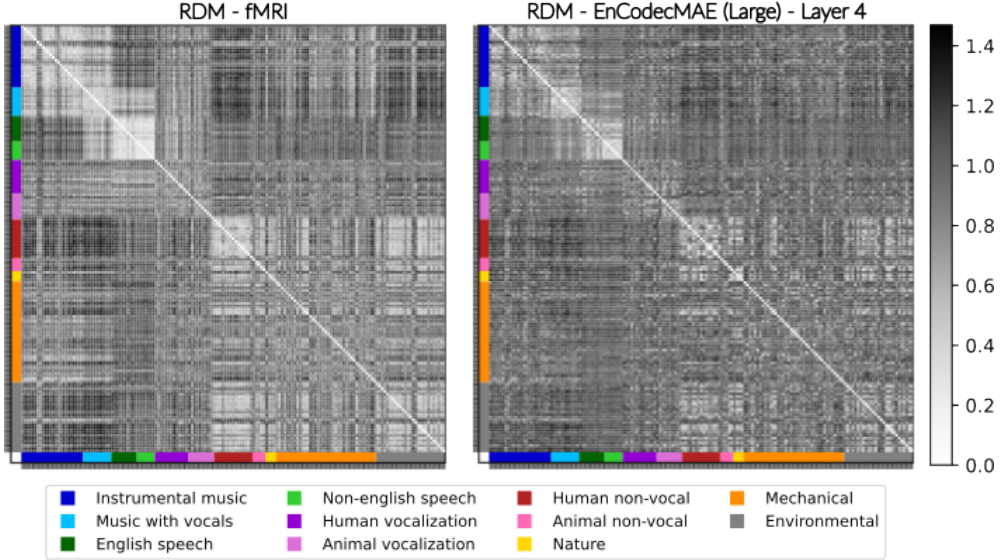


Fig. 3 Example of an RDM computed from NH2015 fMRI responses (left) and from EnCodecMAE Large (right). Rows and columns correspond to the 165 auditory stimuli, grouped by stimulus type as indicated by colors.

($\text{Mel256} \rightarrow \text{EC (LL)}$). Also, consistently with regression results, we do not observe significant differences or clear trends between models that are finetuned or not, and between different iterations of target refinement, except for $\text{Mel256} \rightarrow \text{EC (Large)}$ vs $\text{Mel256} \rightarrow \text{EC (Large + ST)}$, where the refinement leads to a decrease in similarity. Finally, although representations from more recent models like EnCodecMAE and BEATs have the highest ρ_m values, the difference with other models like VGGish or CochResNet50 is not as pronounced as in terms of R_m values from the regression analysis. We believe this difference arises because RSA cannot ignore dimensions in the model representations that are uncorrelated with brain activity. On the other hand, regression analysis can find a subspace of the representation which is relevant for brain activity prediction. In Figure 12 in Section 4.5, we show that although RSA and regression results are highly correlated, the differences are greater than comparing RSA between 2 different datasets (B2021 and NH2015) or methodologies (max layer vs cross-validation).

2.3 Recent models are better predictors of speech and music-related fMRI components

In prior work, an algorithm similar to independent component analysis (ICA) was used to decompose the signal from all voxels into independent components (see Section 4.4). The decomposition is done by first averaging voxel responses over all subjects and then decomposing the resulting matrix of dimension given by the number of stimuli (165) times the number of voxels. Six components in this decomposition explain 80%

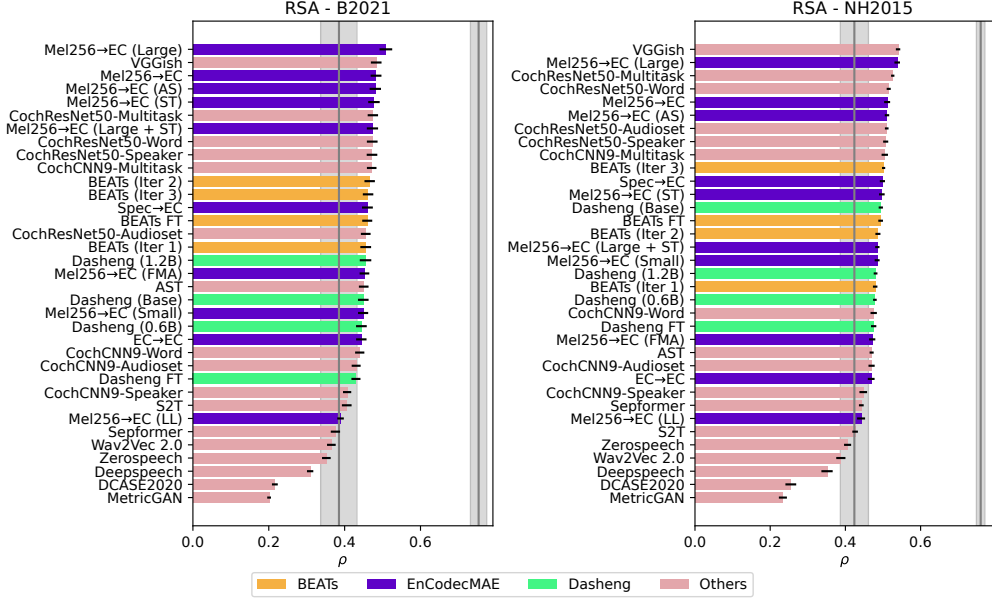


Fig. 4 RSA coefficient, ρ_m , given by the Spearman correlation between brain and model RDMs. Gray lines correspond to the spectro-temporal baseline and the inter-subject RSA topline. Error bars reflect the standard error across subjects.

of the variance in voxel response and they were identified to be selective to low and high frequency tones (LF, HF), broadband spectra, tonal sounds (Pitch), speech, and music. These components can be used as target vector instead of the individual voxel responses in the regression analysis.

This approach has several advantages as it allows us to assess the degree to which models can predict brain activity, separately for each of the components, which are associated to different kinds of stimuli like speech, music or tonal sounds. It also makes the analysis more computationally efficient, as the number of target variables is reduced to six, instead of the number of voxels. A drawback of this analysis is that 20% of the variance in the fMRI signal is not captured by the components, losing some potentially-valuable information. Another limitation is the loss of anatomical specificity compared to voxels, since components are not associated to a particular region in the brain. Further, components are obtained after pooling voxels across participants hence losing the ability to compute subject-specific metrics.

Figure 5 shows the performance of the different audio models in predicting each of the six components. Interestingly, for the first components (related to spectral features such as low and high frequency energy), older models are good predictors, specially those that use cochleagram representations as inputs. In contrast, for components that are selective to speech and music stimuli, the most recent models introduced in this study, which are trained on larger and more diverse datasets using unsupervised objectives and transformer architectures, show superior performance.

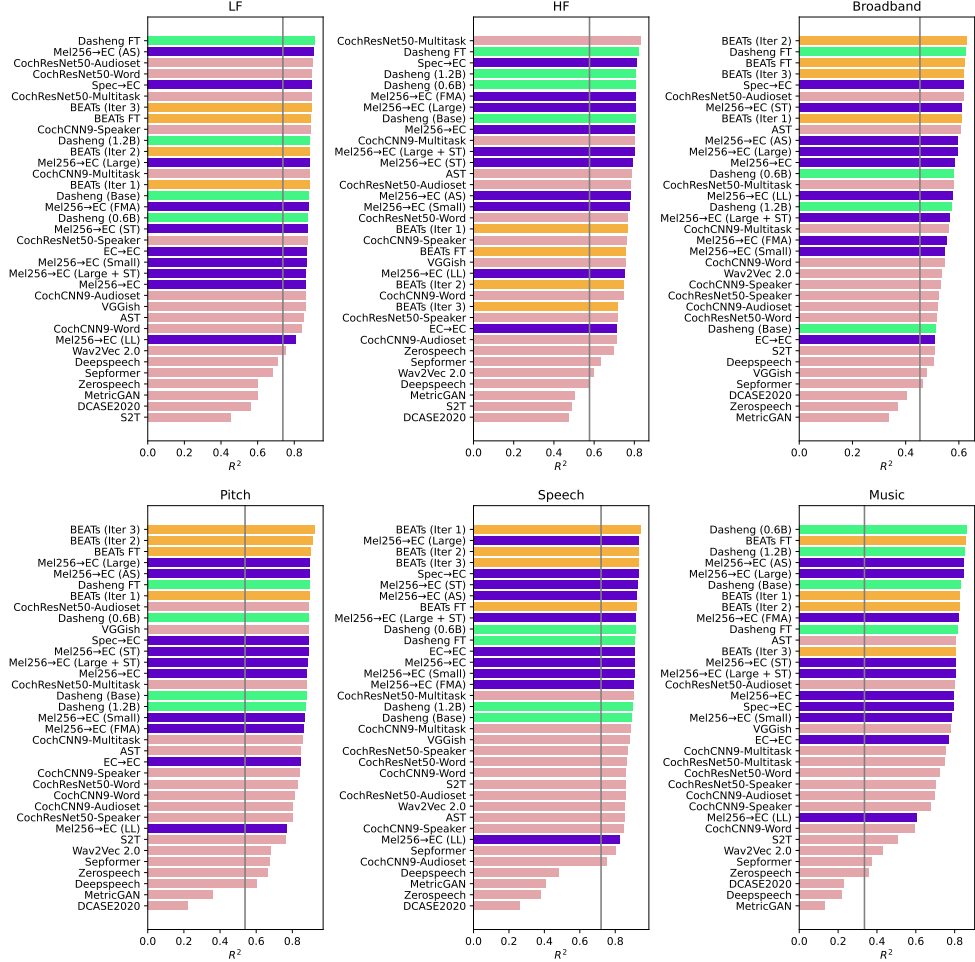


Fig. 5 R^2 values for each of the six components and the audio models evaluated. The gray lines correspond to the spectro-temporal baseline.

Another notable finding is that, contrary to what one might expect, models trained exclusively on speech or music are not the best predictors of the corresponding music and speech selective components. Instead, the top-performing models are those trained on a combination of datasets.

2.4 Brain alignment and model-stage versus brain-region correspondence develop early during pretraining

An interesting question is whether optimizing the pretext task leads the model's representations to become more aligned with those of the auditory cortex. To investigate this, we analyze the Spearman correlation coefficient ρ_m obtained with RSA for model

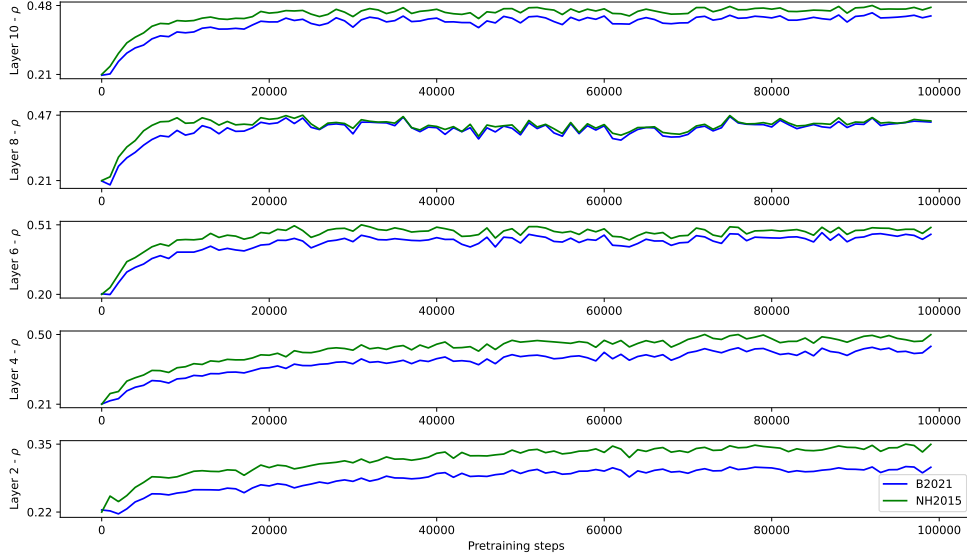


Fig. 6 Spearman’s $\rho_{m,l}$ from the RSA analysis on the B2021 and NH2015 datasets for a subset of layers of EnCodecMAE throughout pretraining.

m as a function of the number of pretraining steps. If the pretext task naturally leads to greater alignment, we should observe an increase in similarity as pretraining progresses. We conducted this analysis using the EnCodecMAE Mel256→EC Base model (see Section 4.2 for more details about the model).

Figure 6 shows that the representations from different layers become increasingly similar to brain representations as pretraining progresses. It is important to note that during pretraining, there is no explicit optimization toward brain similarity, nor is any fMRI-based dataset used. The alignment, much like the strong downstream performance, is a byproduct of the model learning to reconstruct missing audio segments from context.

Interestingly, alignment increases at a higher rate in the last layers compared with the first layers, and also achieve a higher similarity value compared with layer 2. The alignment between audio and brain representations seems to happen early during pretraining. A key finding is that alignment follows remarkably similar patterns across both datasets, despite involving different subjects, indicating the robustness of our methodology.

We also observed that structural differentiation emerges early on, mirroring patterns observed in the auditory cortex. This is illustrated in Figure 7, where layers 7 and 8 exhibit an early decrease in similarity with the primary region, becoming less similar to primary auditory cortex representations than most other layers. In contrast, their similarity with the posterior region remains high and is among the highest across all layers.

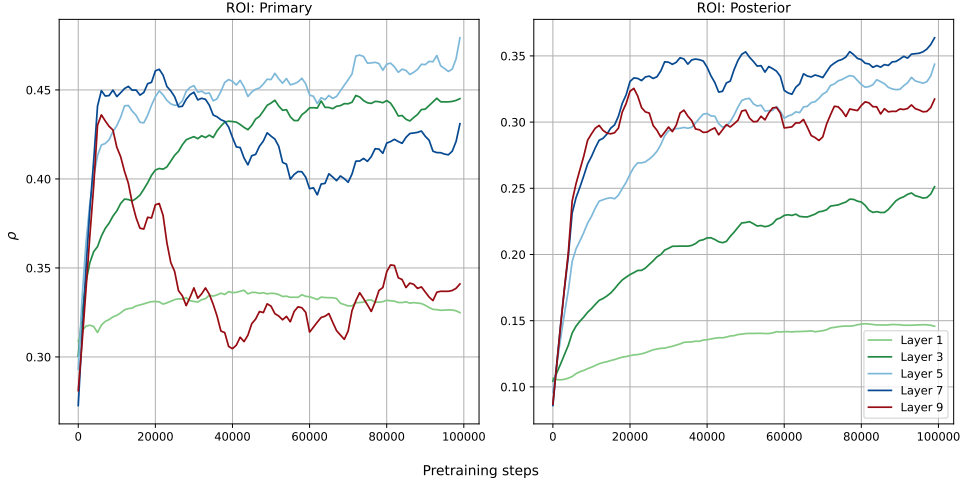


Fig. 7 Evolution in the first 100k pretraining steps of the similarity between audio and brain representations corresponding to the primary and posterior auditory regions in the NH2015 dataset, shown for each layer of the EnCodecMAE model. A Savitsky-Golay smoothing filter with window size=10 and order 3 was applied to the curves for visualization purposes.

Notably, the final layer does not follow the trend observed in earlier layers with respect to primary region similarity, maintaining a high similarity throughout training. We hypothesize that this is due to the pre-post normalization mechanism in EnCodecMAE, which allows it to combine local information from earlier layers. This incorporation of local information may in turn reduce its similarity with the posterior region compared to earlier layers (8 and 9). We do not show the evolution of the ρ values during pretraining for the lateral and anterior regions since they exhibit patterns similar to that of the posterior region shown in Figure 7.

2.5 Downstream task performance correlates with brain alignment

We measured the downstream performance of the different audio models, to determine whether there is a correlation between the representation quality and its alignment with auditory cortex. To assess the representation quality, we followed the HEAREval benchmark protocol:

1. We evaluated in a subset of 6 HEAREval tasks encompassing music, speech and environmental sounds. The tasks are music note classification (NS), music genre classification (GC), speech commands recognition (SC), speech emotion recognition (ER), acoustic event detection (FSD) and acoustic event classification (ESC). These 6 tasks come from well-known datasets in the audio processing community and cover a diverse set of relevant auditory tasks.
2. We used the HEAREval downstream model, which consists of a multi-layer perceptron with limited hyperparameter exploration. Yet, unlike in the standard

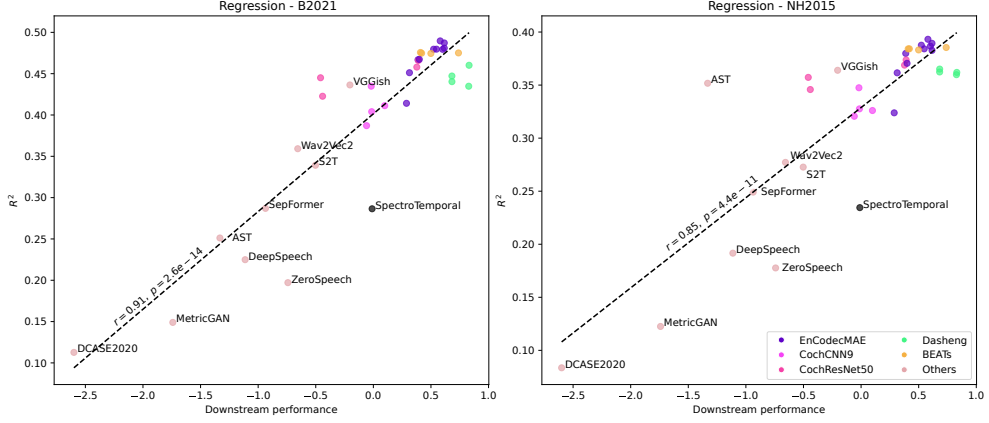


Fig. 8 Overall downstream performance vs R^2 obtained from voxel-wise regression results for the 36 analysed models.

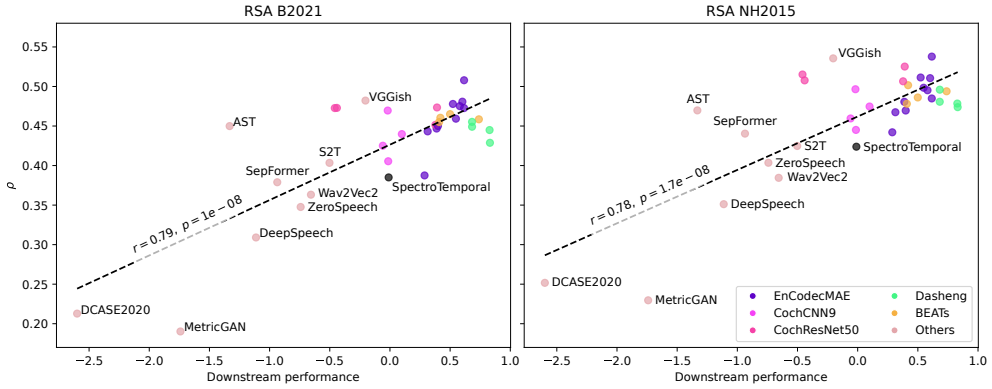


Fig. 9 Overall downstream performance vs Spearman ρ from RSA analysis in B2021 and NH2015 datasets for the 36 analysed models.

HEAREval approach where the last layer of the upstream model is used as input to the downstream model, here we combine the representations from all the layers, so that the procedure is better aligned with how the audio-brain alignment is measured.

3. We obtain a summary metric by calculating z-scores from each task metric and then taking an average over the 6 tasks.

Figure 8 shows that the overall performance metric exhibits a strong positive Pearson correlation ($r = 0.91$ and $r = 0.85$ for B2021 and NH2015 respectively) with R^2 from the regression analysis. Overall, there is a clear trend: models that perform better on downstream tasks also show stronger alignment with the auditory cortex. Even

Method			Music		Speech		Env	FSD	ESC	Overall
			NS	GC	SC	ER				
Regression	NH2015	All	.665	.819	.315	.627	.727	.867		.852
		> -0.75	.410	.511	.269	.408	.678	.690		.728
		All	.672	.747	.567	.657	.858	.776		.907
	B2021	> -0.75	.391	.467	.306	.420	.676	.688		.720
		All	.642	.823	.290	.523	.668	.795		.793
		> -0.75	.391	.477	.121	.173	.472	.470		.517
RSA	NH2015	All	.662	.822	.287	.460	.676	.768		.779
		> -0.75	.458	.506	-.062	.028	.461	.442		.460
		All	.808	.651	.209	.406	.628	.734		.728
	LF	> -0.75	.816	.368	.019	.122	.578	.544		.612
		All	.719	.789	.195	.508	.628	.791		.769
		> -0.75	.640	.547	.087	.250	.568	.564		.665
Regression by Component	Broadband	All	.467	.679	.180	.603	.640	.846		.724
		> -0.75	.249	.410	.303	.477	.782	.753		.727
	Pitch	All	.663	.839	.308	.593	.716	.862		.844
		> -0.75	.282	.570	.149	.342	.678	.684		.670
	Speech	All	.576	.733	.354	.636	.692	.808		.805
		> -0.75	.172	.297	.438	.449	.561	.587		.596
	Music	All	.573	.833	.222	.611	.694	.861		.804
		> -0.75	.420	.609	.200	.422	.712	.711		.763

Table 1 Pearson correlation between the downstream performance for each task and the alignment with the auditory cortex, as measured by voxel-wise and component-wise regression, and RSA. Results shown in green have a significance level $p < 0.01$, in yellow $0.01 \leq p \leq 0.05$ and in red $p > 0.05$. We also show the correlation values for a subset of models with an overall downstream performance higher than -0.75.

when excluding a few poorly performing models (DCASE2020, MetricGAN, DeepSpeech and SepFormer), the correlation remains high and significant ($r = 0.72$ and $r = 0.73$ for B2021 and NH2015 respectively).

Figure 9 presents the same analysis using the ρ value obtained with RSA. The conclusions remain consistent across both types of analysis, showing a clear positive correlation between downstream performance and alignment with the auditory cortex on both datasets.

We also analyzed the correlation between performance on each individual task and the R^2 coefficient from the regression analysis. Results are shown in Table 1, both including all models and filtering out those with an overall score below -0.75. When low-performing models are excluded, speech-related task performance (SC and ER) shows little to no correlation with model-brain alignment. The tasks most strongly correlated with alignment are those related to music genre classification (GC) and acoustic event classification (ESC) and detection (FSD). A possible explanation is that these tasks involve a broader and more diverse set of sounds, potentially engaging a wider range of brain activity patterns. Similar results can be observed while correlating the downstream performance with the RSA metric (ρ).

Table 1 also shows the correlation between the downstream performance and the R^2 value for the different fMRI-derived components. Most tasks show significant correlations with various components. Notably:

- Alignment with the first components (LF and HF), which reflect spectral attributes, correlates strongly with musical note classification performance, while others components show little or no significant correlation for the subset of better-performing systems.
- Alignment with components 3 (Broadband), associated with impulsive (short and broadband) events, and 4 (Pitch), associated with temporally stable sounds, correlate best with the performance on environmental sound tasks.
- Alignment with components 5 and 6, associated with speech and music, respectively, correlate best with the environmental sound classification (ESC) and the overall performance metric.
- The performance of speech-related tasks show the weakest correlation with alignment metrics on all components, which explains why models trained only on speech exhibit the worst alignment. Nevertheless, as expected, the highest correlation for these tasks corresponds to the speech-related component.
- Models that align best with the speech and music components are those that perform well across all tasks, as also shown in Figure 5, where models introduced in this work, which outperform those in the original study, are better aligned with these components.
- The global metric and the FSD task are the only ones with highly significant positive correlations across all components (fully green columns). The FSD task requires detecting a 200 heterogeneous sound classes, suggesting that brain alignment increases with representations that can solve diverse tasks.

The results from these analyses support the Platonic Representation Hypothesis: as audio models improve, their alignment with other top-performing models (like the brain) increases. Also, these findings suggest a practical implication for evaluating audio representations: given the low computational cost of performing representational similarity analysis with fMRI data, these methods could serve as alternatives or complements to benchmarks like HEAREval. For instance, during audio model pre-training, alignment with the auditory cortex could be monitored as a fast and efficient proxy for downstream performance.

3 Discussion

In this study, we analysed the similarity between the representations from 36 different audio models and fMRI measurements by using both regularized linear regression and representational similarity analysis. Moreover, we measured the downstream performance of the audio models in a set of 6 auditory tasks spanning music, speech and environmental sound understanding. This set of measurements allowed us to establish a novel link between the quality of the audio representations, in terms of their usefulness to solve downstream auditory tasks, and their alignment with brain representations. For all the methods we used to measure brain alignment, and for both fMRI datasets, we observed strong positive Pearson correlations between the downstream performance and brain alignment.

We also found that recent models such as EnCodecMAE demonstrate a higher degree of alignment with brain representations compared to earlier models or traditional spectro-temporal baselines, indicating a trend toward biologically plausible representations. Models trained on more diverse datasets (e.g., AudioSet) exhibited greater alignment than those trained solely on speech, suggesting that data diversity during pretraining contributes positively to neural similarity. Our results regarding the correlation between downstream performance and brain alignment explain why these more recent audio models, that also have a good performance in downstream tasks, are better aligned with the brain. Notably, performance on audio tasks such as acoustic event detection and genre music classification showed stronger correlations with brain similarity metrics, and task performance showed distinct correlation with the alignment for specific independent brain components. For instance, note classification performance correlated more strongly with the models alignment to frequency-selective components of primary auditory cortex, while acoustic event detection performance correlated with the alignment to components linked to broadband and tonal spectro-temporal features.

Finally, we showed that brain alignment is a characteristic that emerges early during the pretraining stage of EnCodecMAE, in spite of not optimizing for it. We think that our results support the Platonic Representation Hypothesis, which suggests that as models get better they converge to a common representation, ie. vision and text representations have higher RSA values, or in this case, audio and brain representations have higher similarities. One of the hypothesis of why this happens is that as the models are capable of solving more tasks, the space of possible solutions gets smaller, forcing different models to converge to similar representations, even if modalities are different as they can be seen as different views of the same reality.

3.1 Limitations

Our study is subject to several limitations, particularly regarding the fMRI data. Low temporal resolution of the fMRI measurements (TR = 3.4s) restricts our ability to assess fine-grained temporal encoding, which might be better captured using modalities such as EEG or MEG. The limited number of stimuli (165) also constrains representational diversity, potentially biasing results toward certain pretraining datasets. For example, models trained solely on speech may appear less aligned because the fMRI stimuli included non-speech sounds that the model was not trained to represent.

Moreover, linear regression models may filter out aspects of representations misaligned with brain data, while RSA, although holistic, is sensitive to transformations such as anisotropic scaling. Despite these methodological differences, both analyses yielded consistent findings, lending robustness to our conclusions.

Lastly, the correlation between downstream performance and neural similarity is limited by model coverage. Certain ranges of model performance are underrepresented (e.g., very low-performing models), which may affect correlation strength. Task selection and downstream model design also influence performance metrics and thus the interpretation of alignment. Despite these limitations, we have observed a clear trend in our analysis involving 36 diverse audio models.

3.2 Future directions

One interesting avenue for future work is to repeat our analyses using stimuli restricted to a specific domain, such as speech or music. Public datasets with fMRI recordings of naturalistic speech (e.g., storytelling) could facilitate a more focused evaluation of speech models and their neural alignment. We released the source code and results from this work¹

Additionally, we see an opportunity to build stronger connections between neuroscience and machine learning, by using brain measurements to guide machine learning models. For example, one promising direction is to use fMRI-based RDMs to regularize model training or align audio representations with brain representations. Preliminary work in speech processing [32, 33] suggests that aligning speech models with brain measurements can lead to performance improvements in different auditory tasks.

Another open question is whether alignment with human brain representations is necessary for good downstream performance. Could there exist high-performing models that do not resemble brain activity? Identifying such counterexamples—models with low neural similarity but good task performance, or vice versa—could provide insight into the uniqueness of human-like representations. This connects with the “platonic representations” hypothesis [20], which posits that performance across many tasks may inherently constrain models to converge toward human-like representations. Finding such counter-examples would prove that this theory is incorrect.

Finally, this research invites exploration of neuroconnectionism beyond the human brain. Could models pretrained on animal vocalizations reveal insights about non-human auditory systems? Initial efforts in bird and animal sound modeling [34–36] hint at this possibility, but a more explicit comparison between animal-trained models and animal brain activity remains an exciting direction for future research.

4 Methods

4.1 fMRI datasets and preprocessing

Following Tuckute et al. [16], we used the following 2 fMRI datasets:

- NH2015: This dataset contains fMRI recordings from 8 participants without musical training, all native English speakers aged 19–25 years. During scanning, participants listened to $N = 165$ auditory stimuli, each 2 seconds in duration. The stimuli consisted of everyday sounds, presented in blocks in which each stimulus was repeated 5 times. Each participant completed 3 sessions of approximately 90 minutes, with each session divided into 11 runs comprising 15 stimulus blocks and 4 silent blocks. To monitor attention, one repetition of each stimulus was presented at 7 dB lower intensity than the others, and participants were instructed to press a button whenever this occurred.
- B2021: This dataset contains fMRI recordings from 20 participants, 10 with musical training (8 female, 2 male; mean age = 23.5 years, SD = 3.3; 11–23 years of training) and 10 without musical training (6 female, 4 male; mean age = 25.8 years, SD = 4.1).

¹See <https://github.com/mrpep/braindnn>

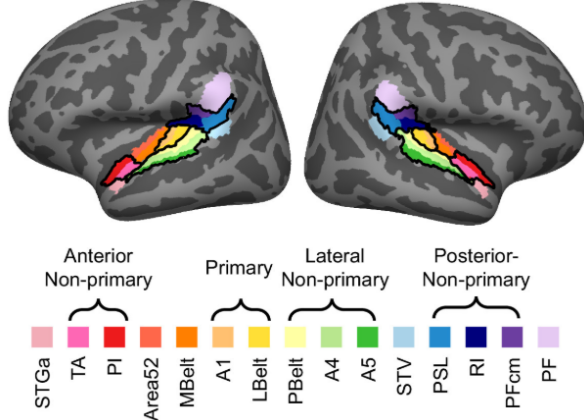


Fig. 10 Anatomical regions following the Glasser parcellation and the grouping considered in [27] included in the fMRI recordings. Figure taken from [27].

The auditory stimuli were identical to those used in NH2015, and the experimental design was similar. The main differences were that each stimulus was repeated 3 rather than 5 times per block, 2 blocks were presented per stimulus (resulting in 6 presentations per session), the experiment was divided into 16 runs, and one stimulus was presented at 12 dB lower intensity than the others to monitor attention.

In both datasets, blood-oxygen-level-dependent (BOLD) responses were recorded with fMRI from voxels within a region of the brain including the auditory cortex, which can be seen in Figure 10. Data were acquired in an orientation parallel to the superior temporal plane, covering the superior temporal gyrus and the superior temporal sulcus. For each session, participant, and stimulus, the first acquisition was discarded. In NH2015, the BOLD response for the remaining four repetitions of each stimulus were averaged, whereas in B2021 a general linear model (GLM) was used instead. The combined signals were converted to percent signal change (PSC) by subtracting and dividing by the voxel's response to silence, and subsequently averaged over time to yield a single scalar response.

For voxel selection, as done by Tuckute et al. [16], we retained those that exhibited significantly greater responses for the stimuli than for silence (t -test, $p < 0.001$) and that responded consistently across sessions. Consistency was quantified for each participant as:

$$r = 1 - \frac{\|v_{12} - \frac{v_3 \cdot v_{12}}{\|v_3\|_2} v_3\|_2}{\|v_{12}\|_2}$$

where, for NH2015, v_{12} denotes a voxel's response to the 165 stimuli averaged over the first two sessions, and v_3 its response in the third session. For B2021, v_{12} corresponds to the responses estimated from the first three repetitions of each stimulus in runs 1–24, and v_3 from the last three repetitions in runs 25–48. Voxels with $r > 0.3$ were included. This selection process is done separately for each subject. This procedure yielded an average of 961.75 voxels per participant (range 637–1221) in NH2015, and

1340 (range 1020–1828) in B2021. Finally, the responses for the selected voxels were averaged across sessions to get a single value per selected voxel per subject.

4.2 Audio models

We expanded the work by Tuckute et al. [16] incorporating different variants of BEATs [21], EnCodecMAE [23] and Dasheng [22], which are more recent general audio models that exhibit a strong performance at different general audio understanding benchmarks. Overall, we analyzed 36 different models, spanning a wide range of model sizes, objectives and audio domains.

- **BEATs** [21] consists of a 12-layer Vision Transformer, pretrained with the Audioset database [37] in a self-supervised way with the pretext task of masked audio modelling (MAM). A fraction (75%) of the melspectrogram input patches are masked and the model is trained to predict discrete labels corresponding to the masked patches using the unmasked ones. In the first iteration, the discrete labels are generated with a random projection tokenizer as in [38]. For the second and third iterations, a tokenizer is trained to discretize the outputs of the previous BEATs iteration, and used to generate the discrete pretraining targets.

We experimented with 4 checkpoints from this model: the final one for each of the 3 iterations, and one where the checkpoint from the third iteration is finetuned with Audioset for acoustic event detection. In all the cases, we extracted 13 sets of activations: the output of each of the 12 transformer layers and the input of the first transformer layer. All the activations have 768 dimensions.

- **Dasheng** [22] is a Masked Autoencoder transformer pretrained with a masked audio modelling task with 272K hours of audio from diverse domains. Instead of using discrete labels as targets, the mean squared error between the reconstructed melspectrogram and the unmasked one is used as a loss.

We experimented with 4 checkpoints from this model: a base model with 86M parameters, 12 layers and 768-dimensional activations; a 0.6B parameters model with 32 layers and 1024-dimensional activations, a 1.2B parameters model with 40 layers and 1536-dimensional activations; and a base model fine-tuned in Audioset for acoustic event detection. For the base models, we extracted embeddings from the output of every transformer layer, while for the 0.6B model we extracted from every 3 layers (1, 4, 7,..., 31) and the last layer (32), and for the 1.2B model we extracted from every 4 layers (1, 5, 9, 13,..., 37) and the last layer (40).

- **EnCodecMAE** [23] is a Masked Autoencoder transformer pretrained with a masked audio modelling pretext task using different datasets. A fraction (50%) of the input frames are masked and the model is trained to predict discrete targets corresponding to the masked segments using the unmasked ones. In a first iteration, discrete labels are obtained from EnCodec [39], a neural audio codec, and in a second iteration, the outputs from the first iteration model are quantized with K-Means and used as targets.

We experimented with 10 different checkpoints:

1. **Mel256→EC (Base)**: first iteration base model with 10 transformer layers and 768-dimensional activations, using melspectrograms as inputs and pretrained

with a mixture of Audioset (AS), LibriLight (LL) and Free Music Archive (FMA). AS contains XX hours of a variety of acoustic events, including some proportion of speech and music. LL consists of 6000 hours of read speech recordings. FMA consists of 800 hours of music.

2. **Mel256→EC (AS)**: same as 1) but pretrained only with AS.
3. **Mel256→EC (LL)**: same as 1) but pretrained only with LL.
4. **Mel256→EC (FMA)**: same as 1) but pretrained only with FMA.
5. **Mel256→EC (Small)**: same as 1) but with only 5 layers and x parameters.
6. **Mel256→EC (Large)**: same as 1) but with 20 layers, x parameters and 1024-dimensional activations.
7. **EC→EC**: same as 1) but using EnCodec features as input.
8. **Spec→EC**: same as 1) but using linear spectrograms as input.
9. **Mel256→EC (Base + ST)**: second iteration of 1).
10. **Mel256→EC (Large + ST)**: second iteration of 6).

For the small and base models, we extracted activations from the output of every transformer layer, while for the large models, we extracted activations from every odd layer (1, 3, 5,..., 19) and the last layer (20).

- **CochDNN** [16] takes as input cochleograms computed using a bank of 211 band-pass filters designed to approximate the response of the human ear. Envelope extraction is performed via a Hilbert transform, followed by a compression stage simulating that of the basilar membrane. The resulting envelopes are then low-pass filtered and downsampled to 200 Hz. Two convolutional architectures, termed CochCNN9 and CochResNet50, were trained on a dataset in which each example consisted of a spoken word embedded in background noise sampled from AudioSet. This setup enabled training on three tasks using the same data: word recognition, speaker identification, and acoustic event detection (based on the background noise). In addition, the authors trained models jointly on the three tasks in a multitask setting. Combining the two architectures with the four objectives resulted in a total of 8 models.

Following Tuckute et al., for CochCNN9 we extracted features from the outputs of the ReLU activations and pooling layers at each convolutional block, leading to 9 sets of activations with shapes ranging from 2304 to 9216 dimensions, and for CochResNet50 we extracted features from the outputs of the first convolutional layer after applying ReLU, the outputs of each ResNet block, and the output of the last average pooling layer, leading to 7 sets of activations with dimensions ranging from 2048 to 14336.

- **AST** [40] is a model that applies a vision transformer to melspectrogram inputs and is trained for acoustic event detection in AudioSet. It is composed of an initial patching and projection layer, which takes the melspectrogram input, splits it into a sequence of 16x16 patches, and projects each of them into 768D vectors. Twelve transformer blocks process this sequence of projected patches and a final linear layer performs the classification into 527 different classes. We extracted embeddings from the output of the patching layer, the 12 transformer blocks, and the final classification layer, leading to 14 sets of activations with 768 dimensions, except for the last layer which has 527 dimensions.

- **VGGish** [41] is an audio classification model that follows the VGG [42] convolutional neural network architecture. The model was trained on the YouTube-100M corpus (70M training videos, 5.24 million hours with 30,871 labels) to predict the video-level labels based on audio information using a cross-entropy loss function. Following Tuckute et al., we extracted representations from the ReLU activation after each convolutional block and dense layer, and from the max-pooling layers. This led to 13 sets of activations having between 128 and 4096 dimensions.
- **DCASE 2020** [43] is a recurrent neural network trained for audio captioning, where the model accepts audio as input and outputs a description of it. We used a model trained in the Clotho dataset [44], which consists of pairs of audios and captions, and was released by the authors. The input to the model is a log-melspectrogram with 64 mel filters, a 23 ms window size, and a 11.5 ms hop size. The model consists of an encoder with 3 bidirectional Gated Recurrent Units (GRU), and a decoder with 1 GRU and an output layer with 4367 neurons corresponding to each unique word in the captions. We extracted activations from the output of every GRU layer and the final output layer, leading to 5 sets of activations with dimensionalities of 512 for the BiGRUs in the encoder, 256 for the decoder GRU and 4367 for the output layer.
- **DeepSpeech 2** [45] is a recurrent neural network trained for automatic speech recognition (ASR). The input to the model is a log-spectrogram, which is processed by two 2D convolutional layers followed by 5 BiLSTM layers and a final fully-connected layer that outputs logits for the 29 classes corresponding to English characters, space, blank and apostrophe. We extracted activations from the 2 convolutional layers and the 5 BiLSTM layers, leading to 7 sets of activations with dimensions ranging from 1312 to 2592.
- **MetricGAN** [46] is a generative adversarial network (GAN) trained for speech enhancement. We used a model trained on the Voicebank-DEMAND dataset [47], which consists of pairs of clean high-quality speech and noise recordings, and is used to train speech enhancement models. The generator consists of 2 BiLSTM layers followed by 2 fully connected layers, while the discriminator is a CNN. The input to the model is a linear spectrogram with a window size of 32 ms and a hop size of 16 ms. We extracted activations from the cell state of the 2 BiLSTM layers and from the outputs of the 2 linear layers, leading to 4 sets of activations with 400 dimensions for the BiLSTM layers, and 300 and 257 dimensions for the linear layers.
- **Wav2Vec 2.0** [48] is a self-supervised speech model pretrained to reconstruct masked segments from speech inputs, and finetuned for ASR. It consists of an initial CNN encoder followed by 12 transformer blocks. Activations were extracted from the CNN encoder output and each of the 12 transformer blocks outputs resulting in 13 sets of activations with 768 dimensions each. We used the base version pretrained and finetuned on the LibriSpeech corpus (960 hours) [49].
- **Sepformer** [50] is a model trained for speech separation with the WHAMR! [51] dataset, and the model estimates optimal masks to separate the speakers from the mixture. The architecture consists of an initial CNN encoder layer, followed by 32 dual-path transformer blocks, which consist of Intra-Transformers modeling short-term temporal dependencies, and Inter-Transformers modeling longer term

dependencies. We extracted activations from the output of the initial encoder layer and every transformer layer, leading to 33 sets of activations with 256 dimensions.

- **S2T** [52] is an encoder-decoder model trained for speech-to-text tasks such as ASR and speech to text translation. The model consists of 2 convolutional layers followed by 12 transformer blocks. We used the checkpoint trained for ASR using LibriSpeech (960h). We extracted activations from the output of the CNN encoder and each transformer layer, leading to 13 sets of activations, each with 1024 dimensions.
- **ZeroSpeech** [53] consists of a Vector-quantized Variational Autoencoder (VQ-VAE), trained for speech reconstruction, and can be used to generate speech in a target speaker’s voice. The encoder is a CNN, while the decoder is a RNN. We only used the encoder, which takes log-melspectrograms as inputs and is followed by 5 1D convolutional layers. We extracted activations from the outputs of every convolutional layer (after ReLU is applied), leading to 5 sets of activations, each with 768 dimensions.
- **Spectro-temporal model** [54] consists of a linear filter bank tuned to spectrotemporal modulations at different frequencies, spectral scales and temporal rates. Spectrotemporal modulation filters were implemented as 2D convolutions with zero padding in frequency (800 samples) and time (211 samples). Filters targeted spectral modulation frequencies of 0.0625–2 cycles/erb and temporal modulation frequencies of 0.5–64 Hz, including both upward and downward sweeps, yielding 96 filters. To capture purely spectral and purely temporal modulations, we added 6 and 8 filters, respectively, for a total of 110. Filter outputs were squared and averaged over time within each frequency channel.

4.3 Voxel response regression

For each subject s and each voxel v , we trained an L2-regularized (ridge) linear regressor to predict its response using the audio representations from layer l of a model m as input. For each model m , subject s , and voxel v , we performed a hyperparameter search to select the regularization strength (α) and the layer (l) to use for prediction. We explored the following α values: [0.01, 0.05, 0.1, 0.5, 1.0, 5.0, 10.0, 50.0]. If the best value of alpha was at the edges (0.01 or 50), we divided or multiplied the best α by 2 until the performance stopped improving, or until α was out of the interval $[10^{-49}, 10^{50}]$. The performance was measured by taking the Pearson coefficient of determination (R^2) between the predicted and true voxel responses. If the Pearson correlation coefficient was less than 0, we set $R^2 = 0$.

We divided the 165 stimuli into 5 equal-size splits. The splits were designed so that they were balanced across the 11 different stimuli categories (mechanical sounds, human vocalizations, human non-vocal sounds, english speech, non-english speech, environmental sound, music, animal vocalizations, animal non-vocal sounds, song and nature sounds). We performed nested cross-validation to select the hyperparameters. That is, for each split, we used the remaining 4 splits to select the hyperparameters using an inner loop of cross-validation. Then, we trained the model in those 4 splits, using the hyperparameter set selected in the inner loop, and predicted the voxel response for the remaining split. This process was repeated until there were predictions for every split. Finally, we obtained the Pearson determination coefficient $R^2_{m,s,v}$.

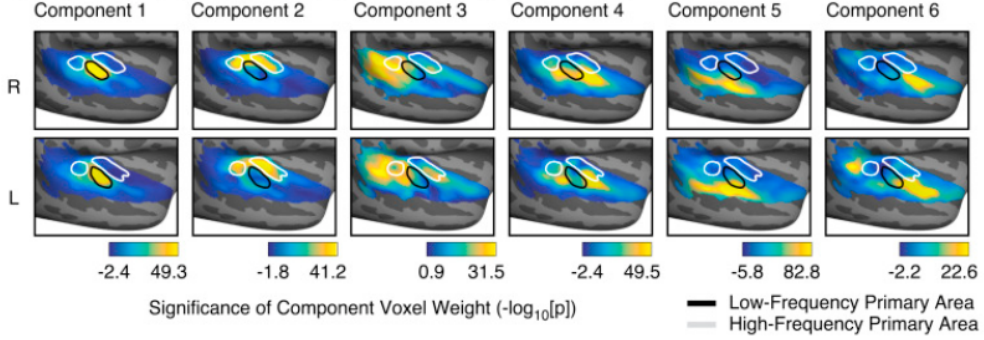


Fig. 11 Weights associated with the independent components identified in [26].

between the voxel response predicted for the 165 stimuli and the fMRI measurements at voxel v of subject s , for audio model m . Finally, in order to get a summary metric for the alignment between each model and all brain measurements, we took the median of all the $R_{m,s,v}^2$ for each subject, leading to $R_{m,s}^2$, and then took the mean across subjects obtaining the final summary metric R_m^2 .

4.4 Component regression

In addition to performing regression directly on voxels, we also regressed onto independent components obtained in a previous study [26]. The decomposition is done by first averaging voxel responses over all subjects and then decomposing the resulting matrix of dimension given by the number of stimuli (165) times the number of voxels. The authors identified six independent components (shown in Fig. 11) that together explained 80% of the voxel variance in the NH2015 dataset. Moreover, the authors were able to characterize the stimulus selectivity of each component:

- **Component 1 (LF)** assigned higher weights to voxels responding to low-frequency pure tones in a tonotopy mapping experiment.
- **Component 2 (HF)** assigned higher weights to voxels responding to high-frequency pure tones.
- **Component 3 (Broadband)** was selective for stimuli with broadband spectra and rapid temporal modulations, exhibiting vertical patterns in a spectrogram.
- **Component 4 (Pitch)** was selective for tonal stimuli, exhibiting horizontal lines in a spectrogram.
- **Component 5 (Speech)** showed strong selectivity for speech, with speech stimuli eliciting the highest responses, followed by sung music and vocalizations.
- **Component 6 (Music)** showed selective responses to music.

For consistency, we report the components in the same order as the original study. Because they were obtained using independent component analysis (ICA), they are not ordered by explained variance, as in PCA. The reported metric is the Pearson coefficient of determination R^2 between the predicted component values and the ones measured from fMRI data.

4.5 Representation similarity analysis

Given a matrix M , a representation dissimilarity matrix (RDM) D can be obtained as

$$D_{ij} = 1 - r(M_i, M_j),$$

with $r(M_i, M_j)$ being a similarity measure between the rows i and j of the M matrix. Following Tuckute et al., we used the Pearson correlation coefficient as a similarity measure, and obtained dissimilarity matrices D_l^a for the audio model responses M_l^a at each layer l , and dissimilarity matrices D_s^b for the voxel responses M_s^b of each subject s . The matrices D_l^a and D_s^b have the same shape $N \times N$ with N being the number of audio stimuli. This consistency in the shape allows to compare dissimilarity matrices coming from representations of different shapes. For comparing the RDMs, the upper triangular matrix elements are extracted and flattened, and Spearman correlation is measured between the resulting vectors yielding a single scalar metric.

The above approach results in a coefficient $\rho_{m,l,s}$ for every subject s and every layer l of the audio model m , which reflects the similarity between the representations obtained from the fMRI of subject s and the representations obtained from the layer l of audio model m . We explored two approaches for obtaining a single similarity measure for the model m :

- **Optimal layer on all data:** we computed the average of $\rho_{m,l,s}$ across subjects, leading to a Spearman correlation coefficient for each layer $\rho_{m,l}$. We finally computed the maximum value across layers as summary metric. This approach is simple but the layer selection is based on the same data which is used for reporting the test metric, which could lead to optimistic results.
- **Optimal layer chosen with cross-validation:** instead of using the $\rho_{m,l,s}$ values computed as above to select the best layer, for each subject we construct an audio RDM D^a performing cross-validation, using the same folds over the stimuli as in the regression analysis. For each fold f_k , we fill the entries $D_{i,j}^a$ corresponding to stimuli $i \in f_k$ and $j \in f_k$, using entries from the RDM matrix corresponding to the best layer l_{best} . The best layer is selected using the entries of the RDM matrices that correspond to stimuli not present in the fold f_k . After computing D^a this way, the ρ value is calculated as above based on this alternative RDM for the model. This method allows reporting a Spearman coefficient on data that was not used to select the best layer, while still using all stimuli for calculating the RDMs. The disadvantage is that the resulting RDMs can contain submatrices coming from different layer RDMs.² In practice, we observed that for most models, the selected layer was consistent across folds and subjects.

In Figure 12 (left), the results using both methods are compared. It can be seen that differences are minimal between both methods, and consequently, we decided to use the simpler method. It can also be seen that these differences are much smaller than those coming from using a different dataset to calculate RSA (Figure 12 (center)), or from using regression instead of RSA as the alignment analysis (Figure 12 (right)).

²Note that this is also the case for the regression analysis where the layer is selected in the inner cross-validation loop before pooling all folds together to compute the final metric.

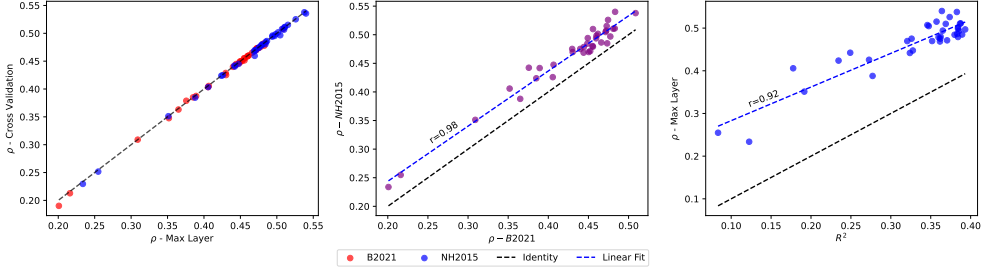


Fig. 12 Left: Comparison between the two analysed methodologies for RSA computation. Mid: Comparison between the RSA results obtained in the B2021 and NH2015 datasets. Right: Comparison between the alignment results obtained in NH2015 using voxel-wise regression and RSA.

In order to obtain RSA values for the primary and posterior regions, as shown in Figure 7, we constructed the fMRI RDM matrices D_s^b using only the subset of voxels corresponding to the anatomical region of interest.

4.6 Audio models performance measurement

In order to measure how good the model representations are for solving audio-related tasks, we evaluated the models in a subset of the HEAREval benchmark [55] tasks:

- **Music note classification:** The NSynth dataset [56] is used, which contains 4-seconds long isolated music notes from different musical instruments. The goal is to predict which note was played among 88 options.
- **Music genre classification:** The GTZAN dataset [57] is used, which contains 30 seconds segments of 1000 different songs, categorized in 10 music genres: blues, classical, country, disco, hiphop, jazz, metal, pop, reggae and rock.
- **Speech commands classification:** The goal is to classify which of 10 possible commands were spoken in a speech segment. Two additional categories are 'noise' and 'other'. The Google Speech Commands Dataset is used.
- **Speech emotion recognition:** The CREMA-D dataset [58] is used, which contains 12 different sentences said by 91 actors with one of the following emotions: anger, disgust, fear, happiness, sadness and neutral, and different emotional intensities. The task consists in classifying the emotion from the speech signal.
- **Acoustic event detection:** The FSD-50K dataset [59] is used, which consists of 100 hours of audios annotated with acoustic events, which can belong to 200 different categories. The task consists in determining which acoustic events happened in an audio segment. As multiple events can occur in a single segment, this is a multilabel classification problem.
- **Environmental sound classification:** the ESC-50 dataset [60] is used, which consists of 2000 5-seconds long recordings of isolated environmental sounds, which can belong to 50 different categories. Some examples of the categories are: rain, dog, baby crying, door slam and helicopter.

We used accuracy as the evaluation metric, except for acoustic event detection, where we used mean average precision (mAP) instead. Together, these tasks assess model performance in diverse domains (speech, music and environmental sounds) using well established datasets.

For each task, we train a downstream classifier that takes the audio representations as input and predicts the corresponding labels. To be consistent with the regression and RSA analysis, we used the representations from the same layers to train the downstream model. Given a set of L representations $\{X_{m,1}, X_{m,2}, \dots, X_{m,L}\}$ from the audio model m , we learn a set of L weights $\{\alpha_1, \alpha_2, \dots, \alpha_L\}$ and obtain a single representation X_m by performing a weighted average of the representations:

$$X_m = \frac{\sum_{i=1}^L |\alpha_i| X_{m,i}}{\sum_{i=1}^L |\alpha_i|}$$

When the representations $X_{m,i}$ have different dimensionalities, we perform Principal Component Analysis (PCA) for each representation and replace $X_{m,i}$ by its first D_{\min} components, where D_{\min} is the smallest dimensionality among the representations. The PCA components are estimated using the downstream task training data.

A multilayer perceptron taking X_m as input is trained jointly with the weights α_i to predict the targets for the task. A small hyperparameter search is performed. Table 2 shows the learning rate, number of hidden layers, and initialization explored, leading to 16 hyperparameter combinations. The search is done using the validation set, when the datasets have train-validation-test splits, and is done in the first fold when the datasets have K cross-validation folds (by using $K - 2$ folds for training, 1 for validation and determining early stopping and 1 for test and determining hyperparameter performance).

Searched hyperparameters	Values
Hidden layers	{1, 2}
Learning rate	{ 3.2×10^{-3} , 1×10^{-3} , 3.2×10^{-4} , 1×10^{-4} }
Initialization	{Xavier Uniform, Xavier Normal}
Fixed hyperparameters	
Dropout	0.1
Normalization	BatchNorm
Hidden activation	ReLU
Hidden neurons	1024

Table 2 Downstream model hyperparameters, following HEAREval benchmark methodology.

Finally, to obtain an overall measure of model performance across tasks, we z-scored metrics within each task and averaged across tasks to compute a single global score.

References

- [1] Doerig, A., Sommers, R.P., Seeliger, K., Richards, B., Ismael, J., Lindsay, G.W., Kording, K.P., Konkle, T., Van Gerven, M.A., Kriegeskorte, N., *et al.*: The neuroconnectionist research programme. *Nature Reviews Neuroscience* **24**(7), 431–450 (2023)
- [2] Güçlü, U., Van Gerven, M.A.: Deep neural networks reveal a gradient in the complexity of neural representations across the ventral stream. *Journal of Neuroscience* **35**(27), 10005–10014 (2015)
- [3] Yamins, D.L., Hong, H., Cadieu, C.F., Solomon, E.A., Seibert, D., DiCarlo, J.J.: Performance-optimized hierarchical models predict neural responses in higher visual cortex. *Proceedings of the national academy of sciences* **111**(23), 8619–8624 (2014)
- [4] Seeliger, K., Fritsche, M., Güçlü, U., Schoenmakers, S., Schoffelen, J.-M., Bosch, S.E., Van Gerven, M.: Convolutional neural network-based encoding and decoding of visual object recognition in space and time. *NeuroImage* **180**, 253–266 (2018)
- [5] Eickenberg, M., Gramfort, A., Varoquaux, G., Thirion, B.: Seeing it all: Convolutional network layers map the function of the human visual system. *NeuroImage* **152**, 184–194 (2017)
- [6] Khaligh-Razavi, S.-M., Kriegeskorte, N.: Deep supervised, but not unsupervised, models may explain it cortical representation. *PLoS computational biology* **10**(11), 1003915 (2014)
- [7] Cadena, S.A., Denfield, G.H., Walker, E.Y., Gatys, L.A., Tolias, A.S., Bethge, M., Ecker, A.S.: Deep convolutional models improve predictions of macaque v1 responses to natural images. *PLoS computational biology* **15**(4), 1006897 (2019)
- [8] Aw, K.L., Montariol, S., AlKhamissi, B., Schrimpf, M., Bosselut, A.: Instruction-tuning aligns llms to the human brain. In: First Conference on Language Modeling
- [9] Goldstein, A., Ham, E., Nastase, S.A., Zada, Z., Grinstein-Dabus, A., Aubrey, B., Schain, M., Gazula, H., Feder, A., Doyle, W., *et al.*: Correspondence between the layered structure of deep language models and temporal structure of natural language processing in the human brain. *BioRxiv*, 2022–07 (2022)
- [10] Kumar, S., Sumers, T.R., Yamakoshi, T., Goldstein, A., Hasson, U., Norman, K.A., Griffiths, T.L., Hawkins, R.D., Nastase, S.A.: Shared functional specialization in transformer-based language models and the human brain. *Nature communications* **15**(1), 5523 (2024)
- [11] Schrimpf, M., Blank, I., Tuckute, G., Kauf, C., Hosseini, E.A., Kanwisher, N.,

Tenenbaum, J., Fedorenko, E.: The neural architecture of language: Integrative modeling converges on predictive processing. *Proceedings of the National Academy of Sciences* **118** (2020)

[12] Güçlü, U., Thielen, J., Hanke, M., Van Gerven, M.: Brains on beats. *Advances in Neural Information Processing Systems* **29** (2016)

[13] Khatami, F., Escabí, M.A.: Spiking network optimized for word recognition in noise predicts auditory system hierarchy. *PLOS Computational Biology* **16**(6), 1007558 (2020)

[14] Millet, J., King, J.-R.: Inductive biases, pretraining and fine-tuning jointly account for brain responses to speech. *arXiv preprint arXiv:2103.01032* (2021)

[15] Vaidya, A.R., Jain, S., Huth, A.: Self-supervised models of audio effectively explain human cortical responses to speech. In: *International Conference on Machine Learning*, pp. 21927–21944 (2022). PMLR

[16] Tuckute, G., Feather, J., Boebinger, D., McDermott, J.H.: Many but not all deep neural network audio models capture brain responses and exhibit correspondence between model stages and brain regions. *Plos Biology* **21**(12), 3002366 (2023)

[17] Mischler, G., Li, Y.A., Bickel, S., Mehta, A.D., Mesgarani, N.: Contextual feature extraction hierarchies converge in large language models and the brain. *Nature Machine Intelligence* **6**(12), 1467–1477 (2024)

[18] Freteault, M., Tetrel, L., Clei, M.L., Bellec, L.P., Farrugia, N.: Alignment of auditory artificial networks with massive individual fmri brain data leads to generalisable improvements in brain encoding and downstream tasks. *Imaging Neuroscience* **3** (2025)

[19] Li, H., Mei, K., Liu, Z., Ai, Y., Chen, L., Zhang, J., Ling, Z.: Refining Self-supervised Learnt Speech Representation using Brain Activations. In: *Interspeech 2024*, pp. 1480–1484 (2024). <https://doi.org/10.21437/Interspeech.2024-604>

[20] Huh, M., Cheung, B., Wang, T., Isola, P.: The platonic representation hypothesis. *arXiv preprint arXiv:2405.07987* (2024)

[21] Chen, S., Wu, Y., Wang, C., Liu, S., Tompkins, D., Chen, Z., Che, W., Yu, X., Wei, F.: Beats: audio pre-training with acoustic tokenizers. In: *Proceedings of the 40th International Conference on Machine Learning*, pp. 5178–5193 (2023)

[22] Dinkel, H., Yan, Z., Wang, Y., Zhang, J., Wang, Y., Wang, B.: Scaling up masked audio encoder learning for general audio classification. In: *Interspeech 2024* (2024)

[23] Pepino, L., Riera, P., Ferrer, L.: EnCodecMAE: leveraging neural codecs for universal audio representation learning. In: *Interspeech 2025*, pp. 3519–3523 (2025).

<https://doi.org/10.21437/Interspeech.2025-506>

- [24] Ylinen, S., Bosseler, A., Junntila, K., Huotilainen, M.: Predictive coding accelerates word recognition and learning in the early stages of language development. *Developmental Science* **20** (2016) <https://doi.org/10.1111/desc.12472>
- [25] Groppe, D.M., Choi, M., Huang, T., Schilz, J., Topkins, B., Urbach, T.P., Kutas, M.: The phonemic restoration effect reveals pre-n400 effect of supportive sentence context in speech perception. *Brain research* **1361**, 54–66 (2010)
- [26] Norman-Haignere, S., Kanwisher, N.G., McDermott, J.H.: Distinct cortical pathways for music and speech revealed by hypothesis-free voxel decomposition. *neuron* **88**(6), 1281–1296 (2015)
- [27] Boebinger, D., Norman-Haignere, S.V., McDermott, J.H., Kanwisher, N.: Music-selective neural populations arise without musical training. *Journal of Neurophysiology* **125**(6), 2237–2263 (2021)
- [28] Lee, S., Chung, J., Yu, Y., Kim, G., Breuel, T., Chechik, G., Song, Y.: Acav100m: Automatic curation of large-scale datasets for audio-visual video representation learning. In: *Proceedings of the IEEE/CVF International Conference on Computer Vision*, pp. 10274–10284 (2021)
- [29] Aw, K.L., Montariol, S., AlKhamissi, B., Schrimpf, M., Bosselut, A.: Instruction-tuning aligns llms to the human brain. *arXiv preprint arXiv:2312.00575* (2023)
- [30] Aw, K.L., Toneva, M.: Training language models to summarize narratives improves brain alignment. In: *International Conference on Learning Representations* (2022). <https://api.semanticscholar.org/CorpusId:257255248>
- [31] Huo, R., Dunbar, E.: Iterative refinement, not training objective, makes hubert behave differently from wav2vec 2.0. In: *Proc. Interspeech 2025*, pp. 261–265 (2025)
- [32] Moussa, O., Klakow, D., Toneva, M.: Improving semantic understanding in speech language models via brain-tuning. *arXiv preprint arXiv:2410.09230* (2024)
- [33] Freteault, M., Le Clei, M., Tetrel, L., Bellec, L., Farrugia, N.: Alignment of auditory artificial networks with massive individual fmri brain data leads to generalisable improvements in brain encoding and downstream tasks. *Imaging Neuroscience* **3**, 00525 (2025)
- [34] Rauch, L., Moummad, I., Heinrich, R., Joly, A., Sick, B., Scholz, C.: Can masked autoencoders also listen to birds? *arXiv preprint arXiv:2504.12880* (2025)
- [35] Moummad, I., Serizel, R., Benetos, E., Farrugia, N.: Domain-invariant representation learning of bird sounds. *arXiv preprint arXiv:2409.08589* (2024)

- [36] Hagiwara, M.: Aves: Animal vocalization encoder based on self-supervision. In: ICASSP 2023-2023 IEEE International Conference on Acoustics, Speech and Signal Processing (ICASSP), pp. 1–5 (2023). IEEE
- [37] Gemmeke, J.F., Ellis, D.P.W., Freedman, D., Jansen, A., Lawrence, W., Moore, R.C., Plakal, M., Ritter, M.: Audio set: An ontology and human-labeled dataset for audio events. In: 2017 IEEE International Conference on Acoustics, Speech and Signal Processing (ICASSP), pp. 776–780 (2017). <https://doi.org/10.1109/ICASSP.2017.7952261>
- [38] Chiu, C.-C., Qin, J., Zhang, Y., Yu, J., Wu, Y.: Self-supervised learning with random-projection quantizer for speech recognition. In: International Conference on Machine Learning, pp. 3915–3924 (2022). PMLR
- [39] Défossez, A., Copet, J., Synnaeve, G., Adi, Y.: High fidelity neural audio compression. arXiv preprint arXiv:2210.13438 (2022)
- [40] Gong, Y., Chung, Y.-A., Glass, J.: Ast: Audio spectrogram transformer. arXiv preprint arXiv:2104.01778 (2021)
- [41] Hershey, S., Chaudhuri, S., Ellis, D.P., Gemmeke, J.F., Jansen, A., Moore, R.C., Plakal, M., Platt, D., Saurous, R.A., Seybold, B., *et al.*: Cnn architectures for large-scale audio classification. In: 2017 Ieee International Conference on Acoustics, Speech and Signal Processing (icassp), pp. 131–135 (2017). IEEE
- [42] Simonyan, K., Zisserman, A.: Very deep convolutional networks for large-scale image recognition. In: 3rd International Conference on Learning Representations (ICLR 2015) (2015). Computational and Biological Learning Society
- [43] Drossos, K., Adavanne, S., Virtanen, T.: Automated audio captioning with recurrent neural networks. In: 2017 IEEE Workshop on Applications of Signal Processing to Audio and Acoustics (WASPAA), pp. 374–378 (2017). <https://doi.org/10.1109/WASPAA.2017.8170058>
- [44] Drossos, K., Lipping, S., Virtanen, T.: Clotho: An audio captioning dataset. In: ICASSP 2020-2020 IEEE International Conference on Acoustics, Speech and Signal Processing (ICASSP), pp. 736–740 (2020). IEEE
- [45] Amodei, D., Ananthanarayanan, S., Anubhai, R., Bai, J., Battenberg, E., Case, C., Casper, J., Catanzaro, B., Cheng, Q., Chen, G., *et al.*: Deep speech 2: End-to-end speech recognition in english and mandarin. In: International Conference on Machine Learning, pp. 173–182 (2016). PMLR
- [46] Fu, S.-W., Yu, C., Hsieh, T.-A., Plantinga, P., Ravanelli, M., Lu, X., Tsao, Y.: Metricgan+: An improved version of metricgan for speech enhancement. In: Interspeech 2021, pp. 201–205 (2021). <https://doi.org/10.21437/Interspeech.2021-599>

- [47] Veaux, C., Yamagishi, J., King, S.: The voice bank corpus: Design, collection and data analysis of a large regional accent speech database. In: 2013 International Conference Oriental COCOSDA Held Jointly with 2013 Conference on Asian Spoken Language Research and Evaluation (O-COCOSDA/CASLRE), pp. 1–4 (2013). IEEE
- [48] Baevski, A., Zhou, Y., Mohamed, A., Auli, M.: wav2vec 2.0: A framework for self-supervised learning of speech representations. *Advances in neural information processing systems* **33**, 12449–12460 (2020)
- [49] Panayotov, V., Chen, G., Povey, D., Khudanpur, S.: Librispeech: an asr corpus based on public domain audio books. In: 2015 IEEE International Conference on Acoustics, Speech and Signal Processing (ICASSP), pp. 5206–5210 (2015). IEEE
- [50] Subakan, C., Ravanelli, M., Cornell, S., Bronzi, M., Zhong, J.: Attention is all you need in speech separation. In: ICASSP 2021-2021 IEEE International Conference on Acoustics, Speech and Signal Processing (ICASSP), pp. 21–25 (2021). IEEE
- [51] Maciejewski, M., Wichern, G., Le Roux, J.: Whamr!: Noisy and reverberant single-channel speech separation. In: Proc. IEEE International Conference on Acoustics, Speech and Signal Processing (ICASSP) (2020)
- [52] Wang, C., Tang, Y., Ma, X., Wu, A., Okhonko, D., Pino, J.: Fairseq s2t: Fast speech-to-text modeling with fairseq. In: Proceedings of the 1st Conference of the Asia-Pacific Chapter of the Association for Computational Linguistics and the 10th International Joint Conference on Natural Language Processing: System Demonstrations, pp. 33–39 (2020)
- [53] Niekerk, B., Nortje, L., Kamper, H.: Vector-quantized neural networks for acoustic unit discovery in the zerospeech 2020 challenge. *Interspeech 2020* (2020)
- [54] Chi, T., Ru, P., Shamma, S.A.: Multiresolution spectrotemporal analysis of complex sounds. *The Journal of the Acoustical Society of America* **118**(2), 887–906 (2005)
- [55] Turian, J., Shier, J., Khan, H.R., Raj, B., Schuller, B.W., Steinmetz, C.J., Malloy, C., Tzanetakis, G., Velarde, G., McNally, K., *et al.*: Hear: Holistic evaluation of audio representations. In: NeurIPS 2021 Competitions and Demonstrations Track, pp. 125–145 (2022). PMLR
- [56] Engel, J., Resnick, C., Roberts, A., Dieleman, S., Norouzi, M., Eck, D., Simonyan, K.: Neural audio synthesis of musical notes with wavenet autoencoders. In: International Conference on Machine Learning, pp. 1068–1077 (2017). PMLR
- [57] Tzanetakis, G., Cook, P.: Musical genre classification of audio signals. *IEEE Transactions on speech and audio processing* **10**(5), 293–302 (2002)

- [58] Cao, H., Cooper, D.G., Keutmann, M.K., Gur, R.C., Nenkova, A., Verma, R.: Crema-d: Crowd-sourced emotional multimodal actors dataset. *IEEE transactions on affective computing* **5**(4), 377–390 (2014)
- [59] Fonseca, E., Favory, X., Pons, J., Font, F., Serra, X.: Fsd50k: an open dataset of human-labeled sound events. *IEEE/ACM Transactions on Audio, Speech, and Language Processing* **30**, 829–852 (2021)
- [60] Piczak, K.J.: Esc: Dataset for environmental sound classification. In: *Proceedings of the 23rd ACM International Conference on Multimedia*, pp. 1015–1018 (2015)